MPC-Based Proactive Swing Attenuation for Double-Pendulum Overhead Cranes

Juhao Su[1,2], Shichen Sun[1,2], Ching-Wei Chang[2], and Siwei Chang[2]

[1]Academy of Interdisciplinary Studies, The Hong Kong University of Science and Technology, Hong Kong S.A.R.
[2]Hong Kong Center for Construction Robotics, Hong Kong S.A.R.

jsuan@connect.ust.hk, ssunbb@connect.ust.hk, ccw@ust.hk, siweichang@ust.hk

Abstract -

Overhead cranes, which are traditionally classified as underactuated systems, face a persistent challenge in balancing the assertiveness of trolley movement and the amplitude of the payload oscillation. This difficulty is exacerbated by the crane's inherent double-pendulum characteristics. To improve the operational efficiency and fault tolerance of cranes when lifting large and heavy construction components, this research proposed a novel and proactive swing attenuation crane controlling approach. The method was designed to integrate two auxiliary control inputs extracted from the complex and coupled dynamics using a customized Model Predictive Controller (MPC). The performance of the proposed approach was validated by comparing it to common controllers such as the linear quadratic regulator (LQR) and sliding mode controller (SMC). It is proven that the proposed approach makes cranes more resilient to specific types of uncertainties and adverse conditions, resulting in safe, efficient, and intelligent overhead crane transportation.

Keywords -

Double-Pendulum; Overhead Crane; Modular integrated Construction (MiC); Swing Attenuation; Proactive Hook-load Stabilization; Model Predictive Control (MPC); Sliding Mode Control (SMC)

1 Introduction

In the Architecture, Engineering, and Construction (AEC) industry, efficient transportation of substantial payloads is a routine necessity, demanding machinery such as crane systems with exceptional maneuverability and adaptability. Recent research highlighted that these crane systems often exhibit the characteristics of underactuated systems, providing increased degrees of freedom with a limited number of control inputs [1], [2], [3]. Consequently, careful treatment of trolley translation in the horizontal plane is crucial to avoid undesirable payload swings, which not only reduce efficiency but also lead to potential on-site damages [4]. In practical applications, the hook is commonly not positioned at the exact end of the hoisting rope; instead, additional ropes connect the load to the hook as shown in Figure 1a. However, this results in a coupled and complex double pendulum swing, making the dynamic model of crane-load challenging to control [5].

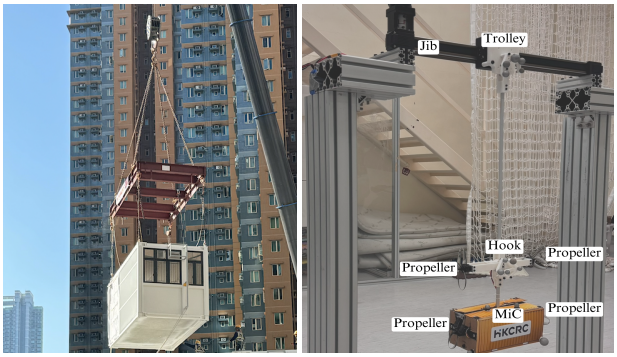

(a) Demonstration of connection between hook and MiC (b) The self-built 2-D overhead crane model

Figure 1. Onsite photos of MiC and 2-D crane model

Traditionally, skilled operators effectively mitigate load oscillations based on their environmental perception and empirical judgment. However, given the substantial costs associated with workforce training and potential accidents during manual crane operations, there is a compelling need for advanced automated control mechanisms tailored for crane systems or a novice-friendly auxiliary operating system, especially for transporting giant and heavy payloads like MiC modules [6].

The pendulum model poses a classical oscillatory control problem, prevalent in all cranes. Previous researchers have applied various open-loop control methods to eliminate hook swings. Two common strategies include input shaping [7], [8] and trajectory planning-based control [9], [10]. These methods design multiple inputs based on the system's dynamic model to counteract oscillations. However, vulnerability may arise if the system identification during modeling is incomplete, or if unknown external disturbances occur during execution [11]. In such cases, aligning the system's response with the envisioned motion trajectory becomes challenging. Concurrently, numerous

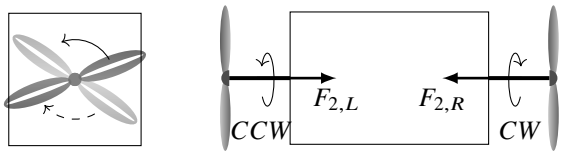

(a) Side-view (b) Front-view

Figure 2. Illustration of spinning propellers mounted on the MiC block (CW for clock-wise, CCW for counter-clock-wise), total force acted on the block would be $F_2 = F_{2,L} - F_{2,R}$, where the propellers mounted on the hook were identical

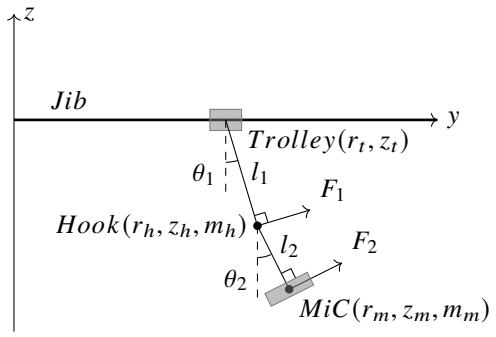

Figure 3. Schematic of the double-pendulum system

studies have explored closed-loop control, employing advanced controllers like Fuzzy Control and its variant [12], [13], [14], as well as Model Predictive Control (MPC) [15], [16]. These controllers effectively mitigate swing angles in both transient and steady-state phases. However, when the model is intricately delineated as a double pendulum, the pronounced nonlinear dynamics pose challenges, especially considering external factors like air resistance and wind, which could compromise the reliability of the controller's model. Despite adopting a closed-loop methodology, the scarcity of controllable variables in underactuated systems remains a regrettable limitation.

Therefore, to enable rapid and significant oscillation suppression during various trolley movement tasks, a novel approach adding two sets of auxiliary control inputs is introduced to this underactuated system. Given the strong coupling behavior among inputs and dynamics, the application of single-input single-output (SISO) controllers, such as ordinary PID controllers, may encounter challenges [17]. This study emphasizes the application of multi-input multi-output (MIMO) controllers instead, for achieving desired control outcomes.

Maintaining the integrity of the system, the aforementioned control inputs rely on the thrust differentials generated by propellers' rotations, as both the hook and MiC are suspended in the air and connected using flexible cables and joints, without moment transmission. This configuration, as illustrated in Figure 1b and 2, allows for the desired execution of intended objectives meanwhile minimizing response instability and lag during swing angle zero-crossing transitions, where the need for abrupt stop-reverse rotations of propellers arises. Since an overhead crane involves movements in two perpendicular planes [18], the study formulates a 2-D spatial model for preliminary validation and presents the following contributions:

1. Analyze the system dynamics of a 2-D overhead crane with two additional control inputs.
2. Utilizing states of the hook and measurable trolley movement, design a model predictive-based controller to tune the inputs under constraints.
3. Achieve noticeable efficacy and show strong resilience against assigned adverse impacts and uncertainty through simulations.

The rest of the paper is organized as follows. Section 2 analyzes full-state dynamics for controller design under the hypothesis of single-axis trolley movement along the jib and forces acting at the center of mass. Simulations in Section 3 verify performance and robustness. The conclusion and future work are presented in the last section.

2 Methodology

2.1 System dynamics

For the 2-D overhead crane scenario interested in this study, its schematic is shown in Figure 3, all directions and angular polarity are specified and applied consistently throughout all simulations and controller designs. If the first set of steel ropes connecting the trolley and the hook is l_1, the second set connecting the hook and MiC block is l_2, then all coordinates can be properly expressed using $r_t, \theta_1, \theta_2, l_1, l_2$, and trigonometry as:

$$r_h = r_t + l_1 sin\theta_1, \quad r_m = r_t + l_1 sin\theta_1 + l_2 sin\theta_2,$$
$$z_h = 0 - l_1 cos\theta_1, \quad z_m = 0 - l_1 cos\theta_1 - l_2 cos\theta_2.$$

Then the dynamics of this system can be represented using Lagrangian Mechanics. The kinetic energy ($\mathscr{T}$), potential energy ($\mathscr{V}$) and Lagrangian ($\mathscr{L}$) of the system can be expressed as below:

$$\begin{aligned}\mathscr{T} = &\frac{1}{2} m_m((\dot{r}_t + l_1 \cos\theta_1\dot{\theta}_1 + l_2 \cos\theta_2\dot{\theta}_2)^2 \\ &+ (l_1 \sin\theta_1\dot{\theta}_1 + l_2 \sin\theta_2\dot{\theta}_2)^2) \\ &+ \frac{1}{2} m_h((\dot{r}_t + l_1 \cos\theta_1\dot{\theta}_1)^2 + l_1^2 \sin\theta_1^2\dot{\theta}_1^2),\end{aligned} \tag{1}$$

$$\mathscr{V} = -m_m g(l_1 \cos\theta_1 + l_2 \cos\theta_2) - m_h g l_1 \cos\theta_1, \tag{2}$$

$$\mathscr{L} = \mathscr{T} - \mathscr{V}. \tag{3}$$

For the forces acting on the hook and MiC block, they are marked as F_1 and F_2, respectively. Since their directions are always perpendicular to the rope sets (l_1, l_2) and within the plane of y-z axes, their interference against θ_1 and θ_2 can be derived as below:

$$\frac{\mathrm{d}}{\mathrm{d}t}\frac{\partial \mathscr{L}}{\partial \dot{\theta}_1} - \frac{\partial \mathscr{L}}{\partial \theta_1} = F_1 l_1, \tag{4}$$

$$\frac{\mathrm{d}}{\mathrm{d}t}\frac{\partial \mathscr{L}}{\partial \dot{\theta}_2} - \frac{\partial \mathscr{L}}{\partial \theta_2} = F_2 l_2, \tag{5}$$

substituting (3) to (4) and (5), the shortened form can be obtained:

$$\begin{aligned} F_1 = {} & l_1(m_h + m_m)\ddot{\theta}_1 + (m_h + m_m)\cos\theta_1 \ddot{r}_t \\ & + (m_h + m_m)g\sin\theta_1 + l_2 m_m \sin(\theta_1 - \theta_2)\dot{\theta}_2^2 \\ & + l_2 m_m \cos(\theta_1 - \theta_2)\ddot{\theta}_2, \end{aligned} \tag{6}$$

$$\begin{aligned} F_2 = {} & l_2 m_m \ddot{\theta}_2 + m_m \cos\theta_2 \ddot{r}_t + m_m g \sin\theta_2 \\ & - l_1 m_m \sin(\theta_1 - \theta_2)\dot{\theta}_1^2 + l_1 m_m \cos(\theta_1 - \theta_2)\ddot{\theta}_1. \end{aligned} \tag{7}$$

2.2 Linearization and state-space function

For crane dynamics, independent of the categories they belong to, a widely adopted and well-established practice is to linearize the dynamic equations through the small angle assumption [19], [20]. For Equation (6) and (7), they can be linearized and rearranged as below:

$$\begin{aligned} \ddot{\theta}_1 = {} & -\frac{g(m_h + m_m)}{l_1 m_h}\theta_1 + \frac{g m_m}{l_1 m_h}\theta_2 - \frac{F_2 - m_m \ddot{r}_t}{l_1 m_h} \\ & + \frac{F_1 - (m_h + m_m)\ddot{r}_t}{l_1 m_h}, \end{aligned} \tag{8}$$

$$\begin{aligned} \ddot{\theta}_2 = {} & \frac{g(m_h + m_m)}{l_2 m_h}\theta_1 + \frac{(m_h + m_m)(F_2 - m_m \ddot{r}_t)}{l_2 m_h m_m} \\ & - \frac{F_1 - (m_h + m_m)\ddot{r}_t}{l_2 m_h} - \frac{g(m_h + m_m)}{l_2 m_h}\theta_2. \end{aligned} \tag{9}$$

The primary objective of the controllers is to mitigate the oscillations of both the hook and MiC module near the normal projection of the trolley position. Thus, the full states vector in this study will be designated as $x(t) = [\theta_1, \dot{\theta}_1, \theta_2, \dot{\theta}_2]^T$ and the desired state should be $x_{des} = [0, 0, 0, 0]^T$. Inspired from Equation (8) and (9), let

$$\upsilon_1 = F_1 - (m_h + m_m)\ddot{r}_t, \tag{10}$$

$$\upsilon_2 = F_2 - m_m \ddot{r}_t, \tag{11}$$

thus a tailored control inputs vector $u(t) = [\upsilon_1, \upsilon_2]^T$ can be obtained to form the following state-space system:

$$\dot{x} = Ax + Bu, \tag{12}$$

$$y = x, \tag{13}$$

where $y(t) \in \mathbb{R}^{4\times 1}$ denotes the output vector, $A \in \mathbb{R}^{4\times 4}$ and $B \in \mathbb{R}^{4\times 2}$ are the system parameter matrices, where can be derived from Equation (8) - (13) as below:

$$A = \begin{bmatrix} 0 & 1 & 0 & 0 \\ -\frac{g(m_h+m_m)}{l_1 m_h} & 0 & \frac{g m_m}{l_1 m_h} & 0 \\ 0 & 0 & 0 & 1 \\ \frac{g(m_h+m_m)}{l_2 m_h} & 0 & -\frac{g(m_h+m_m)}{l_2 m_h} & 0 \end{bmatrix}, \tag{14}$$

$$B = \begin{bmatrix} 0 & 0 \\ \frac{1}{l_1 m_h} & -\frac{1}{l_1 m_h} \\ 0 & 0 \\ -\frac{1}{l_2 m_h} & \frac{m_h+m_m}{l_2 m_h m_m} \end{bmatrix}. \tag{15}$$

It is worth noting that $\ddot{r}_t$ is neither an independent control input nor a component of the system states. Given that the trolley movement is considered arbitrary, acceleration serves as a parameter readily obtainable through measurement. They could be treated as compensation in the controller for the dynamic impact of external motion on the system output.

Take a time interval T_s as sampling time, the system can be properly discretized from Equation (12) and (13):

$$x(k+1) = A_d x(k) + B_d u(k), \tag{16}$$

$$y(k) = x(k), \tag{17}$$

where $A_d = (1 + AT_s)|_{x=x(k)}$, $B_d = (BT_s)|_{x=x(k)}$.

2.3 MPC design

Model Predictive Controller (MPC), employing the receding horizon approach, is a control strategy that predicts the dynamics within h steps (horizon length) and optimizes the control input array to minimize the cost between predicted and reference values. Eventually, only the first element of this array is applied. Therefore, a reference generator for prediction at time instant k within the horizons is set as:

$$r_f(k)_i = x(k)_1 + (i-1)\frac{x_{des} - x(k)_1}{h-1}, \quad i = 1, 2, 3, \ldots, h, \tag{18}$$

where $r_f(k)_i$ is the i^{th} generated reference state at time instant k, $x(k)_1$ denotes state at time instant k, and the discretized system follows:

$$x(k)_i = x(k)_{i-1} + (\frac{T_d}{h} + T_s)\dot{x}(k)_{i-1}, \quad i = 2, 3, 4, \ldots, h, \tag{19}$$

where T_d is the inherent time delay of the system, T_s is the time step for prediction, and the cost function is defined

as:

$$J_M = (r_f(k)_h - x(k)_h)^T F_M (r_f(k)_h - x(k)_h) + \sum_{i=1}^{h-1} \{(r_f(k)_i - x(k)_i)^T Q_M (r_f(k)_i - x(k)_i) + u_i^T R_M u_i\}, \tag{20}$$

where $Q_M \in \mathbb{R}^{4\times4}$, $F_M \in \mathbb{R}^{4\times4}$ and $R_M \in \mathbb{R}^{2\times2}$ denotes weight matrices for tuning control preference on process error, final error, and control effort, respectively.

One leading advantage of adopting MPC lies in its ability to impose constraints not only on the generation of the system's output but also on the state variables in upcoming time steps. The constraints on input selection typically relate to the mechanical capabilities of the device, such as acceleration limit and jerk limit, while the state constraint prevents the system from exceeding undesirable states regarding safety. In this study, the quadratic programming (QP) problem with constraints was defined as:

$$\begin{aligned} min \quad & J_M \\ s.t. \quad & \dot{x} = f(x(t), u(t)) \\ & |\theta_i| \le \theta_{max}, \quad i = 1, 2 \\ & u(t) \in \Upsilon(t), \end{aligned} \tag{21}$$

where $f(\cdot)$ denotes the predict function and can be discretized into Equation (19) and further derived by substituting Equation (8) and (9), Υ represents the input constraints including jerk and acceleration according to motor limitation.

Conservatively setting these constraints can mitigate actuator saturation in hardware experiments [18], which enables MPC to more effectively anticipate future state changes in a well-defined dynamic system.

3 Simulations

3.1 Comparative controller design

3.1.1 LQR

According to the state-space derived in Section 2.2, a Linear Quadratic Regulator (LQR) can be established using Equation (16) and (17). A standard LQR cost function is introduced as below:

$$J_L = \sum_{i=0}^{\infty} \{(x_{curr} - x_{des})^T Q_L (x_{curr} - x_{des}) + u^T R_L u\}, \tag{22}$$

where $(x_{curr} - x_{des})$ denotes the error between the current state and desired state, $u = -K_{lqr}(x_{curr} - x_{des})$, $Q_L \in \mathbb{R}^{4\times4}$ and $R_L \in \mathbb{R}^{2\times2}$ denote two weight matrices for precision and control effort trade-off. An optimum coefficient K_{lqr} can be then obtained from solving the optimizing problem of $min\ J_L$ and implemented to compute the optimal control vector as a constant matrix.

3.1.2 SMC

Sliding Mode Controller (SMC) employs a sliding surface, which is a hyperplane in the space constituted of state error and its derivative, and utilizes discontinuous control to make the system slide towards this plane and converge towards the origin of the space, which implies no state error exists and so as the trend it induces. Let $x_s(t) = [\theta_1, \theta_2]^T$, control objective is $x_{s,des} = [0, 0]^T$ and let

$$\ddot{x}_s = \delta + \Lambda u, \tag{23}$$

where δ and Λ can be derived from Equation (8) and (9) as:

$$\delta = \begin{bmatrix} -\frac{g(m_h+m_m)}{l_1 m_h}\theta_1 + \frac{g m_m}{l_1 m_h}\theta_2 \\ \frac{g(m_h+m_m)}{l_2 m_h}\theta_1 - \frac{g(m_h+m_m)}{l_2 m_h}\theta_2 \end{bmatrix}, \tag{24}$$

$$\Lambda = \begin{bmatrix} \frac{1}{l_1 m_h} & -\frac{1}{l_1 m_h} \\ -\frac{1}{l_2 m_h} & \frac{m_h+m_m}{l_2 m_h m_m} \end{bmatrix}. \tag{25}$$

Set the sliding mode function as

$$s(t) = \Omega(x_s - x_{s,des}) + (\dot{x}_s - \dot{x}_{s,des}), \tag{26}$$

where $\Omega = \mathrm{diag}[\varpi_1, \varpi_2]$ must satisfy Hurwitz condition of $\varpi_1 > 0, \varpi_2 > 0$,

$$\dot{s} = \Omega(\dot{x}_s - \dot{x}_{s,des}) + (\ddot{x}_s - \ddot{x}_{s,des}), \tag{27}$$

$$\dot{s} = -\epsilon tanh(s) - \rho s, \tag{28}$$

where Equation (28) is the defined expression to achieve a nearly exponential reaching law toward the sliding plane with $\epsilon > 0$, $\rho > 0$ so that the Lyapunov function meets its criterion:

$$V = \frac{1}{2}s^2 \ge 0,$$
$$\dot{V} = s\dot{s} \le 0.$$

From Equation (23) - (28), the control input u of SMC could be derived as:

$$u = (\Lambda^T\Lambda)^{-1}(\Lambda^T(\delta + \Omega(\dot{x}_s - \dot{x}_{s,des}) - \epsilon tanh(s) - \rho s). \tag{29}$$

3.2 Comparative simulation results

To validate the effectiveness of proposed proactive control method and the designed controller, a comparative software in the loop (SITL) simulation is conducted using MATLAB & Simulink by creating non-linear dynamic model plant based on Equation (6) and (7), the constant

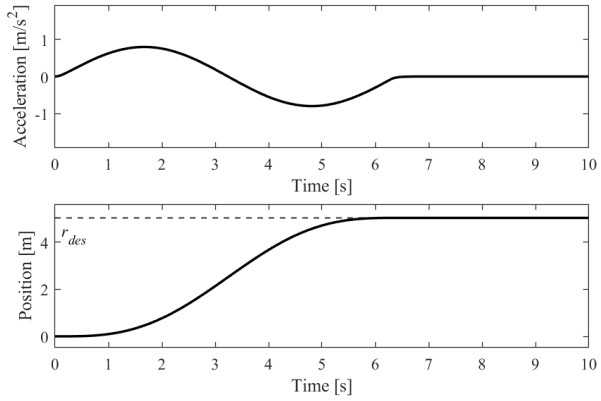

Figure 4. Trolley movement pattern

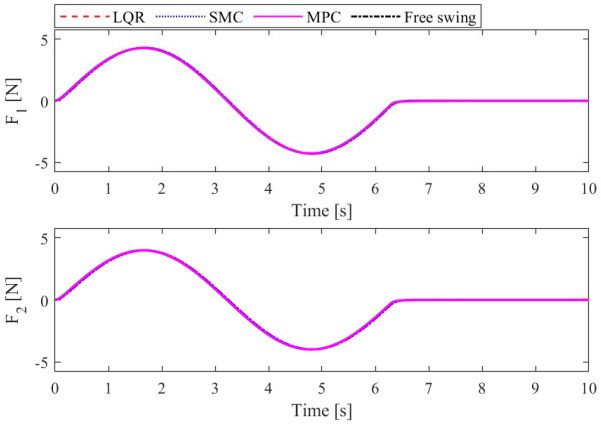

Figure 5. Simulation result of applied force (F_1, F_1)

parameters introduced in the preceding formula derivation will be assigned according to the actual measurements from the model in Figure 1b to aids experiments in the future:

$$m_h = 0.38\ [\text{kg}], \quad l_1 = 0.6\ [\text{m}], \quad g = 9.81\ [\text{N/kg}],$$
$$m_m = 4\ [\text{kg}], \quad l_2 = 0.2\ [\text{m}].$$

3.2.1 Ideal condition

The simulated scenario began at time instant $t = 0[s]$ with the initial condition of staying at equilibrium. Meanwhile, a smooth initiation was provided for the trolley with starting jerk $\dddot{r}_t = 0$ by applying a first-order low-pass filter to a sinusoidal acceleration as shown in Figure 4. The trolley continued its motion until $t = 2\pi[s]$, reaching its desired position r_{des}. Throughout the trolley's motion and after the motion terminated, each controller was aimed to minimize the oscillations in the angles θ_1 and θ_2.

The simulated configuration for all controllers is identical, all the sampling frequencies were set to be $100[Hz]$,

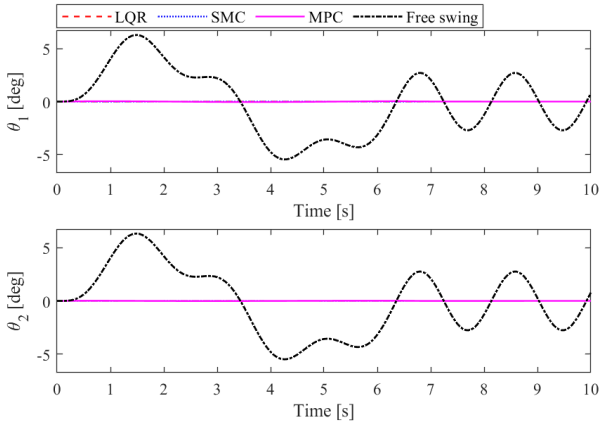

Figure 6. Simulation result of swing angle (θ_1, θ_2)

and the T_s in MPC was set to be $0.05[s]$ with horizon $h = 10$.

The LQR weight matrices and coefficients in SMC were fixed to

$$Q_L = \text{diag}[5, 0.2, 5, 0.2], \quad \epsilon = 15, \quad \rho = 150,$$
$$R_L = \text{diag}[5 \times 10^{-3}, 5 \times 10^{-3}], \quad \Omega = \text{diag}[2, 4],$$

as both LQR and SMC rely on state-space where u is not directly equivalent to the applied force, the compensation of $\ddot{r}_t$ term according to Equation (10) and (11) is needed:

$$F_1 = \upsilon_1 + (m_h + m_m)\ddot{r}_t, \tag{30}$$
$$F_2 = \upsilon_2 + (m_m)\ddot{r}_t. \tag{31}$$

Weight matrices in MPC are defined as:

$$Q_M = \text{diag}[5, 0.18, 5, 0.18],$$
$$F_M = \text{diag}[10, 1, 10, 1],$$
$$R_M = \text{diag}[1 \times 10^{-7}, 1 \times 10^{-7}],$$

and the OCP in (21) is solved by a multi-shooting method with each time interval solved by an interior point optimizer (IPOPT) within CasADi [21].

To avoid transient and excessively high outputs, all forces are constrained by a saturation module within the threshold of $|F_1|, |F_2| \leq 5[N]$. The performance of different controllers was evaluated by observing swing angle θ_1 and θ_2 as shown in Figure 6.

The results indicate that the proposed proactive approach with different controllers can make the system keep a near equilibrium during the acceleration and deceleration of the trolley. This reduction brings the oscillations from potentially hazardous angles ($6.5[deg]$) to virtually $0[deg]$. According to Figure 5, after the trolley moved, the forces are dominated by the compensation term of $\ddot{r}_t$ instead of states, therefore exhibiting subtle distinctions among different controller behaviors.

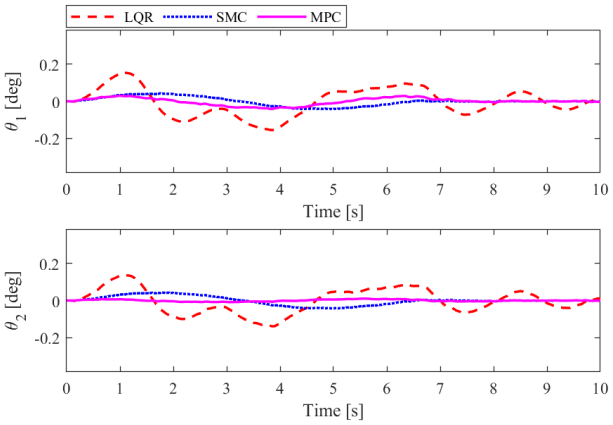

Figure 7. Swing angle (θ_1, θ_2) with $0.02[s]$ delay

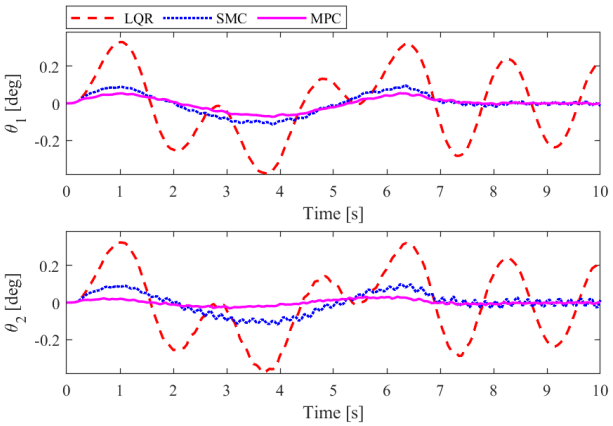

Figure 8. Swing angle (θ_1, θ_2) with $0.04[s]$ delay

3.2.2 Condition with delay and noise

However, trolley acceleration ($\ddot{r}_t$) obtained from sensors may have delay and noise, so as the states obtained. Thus in this group of tests, the signal transport delay is considered and the noise in the sensors is simulated by adding Gaussian noise to the original states vector $x(t)$ and $\ddot{r}_t$:

$$N(t) = [\theta_1, \dot{\theta}_1, \theta_2, \dot{\theta}_2, \ddot{r}_t]^T + n, \tag{32}$$

where $n = [n_1, n_2, n_3, n_4, n_5]^T \sim \mathcal{N}(0, \sigma_i)$ is a vector that each element is independent and identically distributed Gaussian random variables with a mean of zero and follow a normal distribution with standard deviation σ_i, given the magnitude of n_{1-4} is on the order of 10^{-6} and n_5 is on the order of 10^{-4}.

Since the latency is not a constant and instead, fluctuates around a baseline. To illustrate this, the signal delay is modeled as the sum of a constant part and a random variable with a variance of 0.2. The T_d of MPC in Equation (19) can only access the constant part of the delay and is unaware of the current magnitude of the random component.

After some preliminary numerical simulations, LQR and SMC exhibited substantial oscillations and signs of non-convergence in the presence of delay, leading to the implementation of fractional gains to u (K_1 for LQR, K_2 for SMC), the applied forces are in the form below:

$$F_{1,fi} = \upsilon_1 K_i + (m_h + m_m)\ddot{r}_t, \tag{33}$$

$$F_{2,fi} = \upsilon_2 K_i + (m_m)\ddot{r}_t, \; i = 1, 2. \tag{34}$$

Table 1. Quantified results with increased m_m

Method	$\theta_{1,max}$	$\theta_{2,max}$	$\theta_{1,RMSE}$	$\theta_{2,RMSE}$
LQR	-2.38	-2.27	0.86	0.78
SMC	-2.40	-2.23	0.85	0.81
MPC	-1.31	-1.42	0.78	0.84

Through iterative adjustments, these gains were eventually set at critical values where the controllers were prone to collapse, as outlined below:

$$\text{delay} = 0.02[s], \quad K_1 = 0.2, \quad K_2 = 0.25,$$
$$\text{delay} = 0.04[s], \quad K_1 = 0.04, \quad K_2 = 0.05.$$

The data depicted in Figures 7 and 8 illustrates the impact of introducing delay and noise on controller performance. However, with the aid of fractional gain, it does not lead to a severe failure. Notably, LQR exhibits high sensitivity, with decreasing gain causing the persistent squeezing of state effects. It fails to achieve state convergence as the delay continues to increase. In comparison, SMC outperforms LQR, showcasing its resilience to uncertainty and achieving a considerable extent of convergence. MPC emerges as the most trustful option, requiring no adjustment like fractional gains. It exhibits only minor fluctuations in the vicinity of the zero axis.

However, the capacity of LQR and SMC to control pure state changes is significantly diminished by the fractional gain, particularly in facing unknown disturbances directly affecting the load and hook.

3.2.3 Condition with actuator saturation

According to the findings presented in Figure 6, the supplied forces F_1 and F_2 already approached the assumed actuator limit, and further increment may lead to actuator saturation. Therefore, the MiC mass (m_m) was modified to $8[kg]$, while maintaining the output saturation operative within the range of $[-5, 5][N]$ to test the saturated performances. Before initiating the simulation, the input constraints (Υ) of the MPC are defined as:

$$|F_i| \leq 5, \quad i = 1, 2. \tag{35}$$

However, Equation (30) and (31) imply that adjustments applied to the LQR and SMC weight matrices affect the

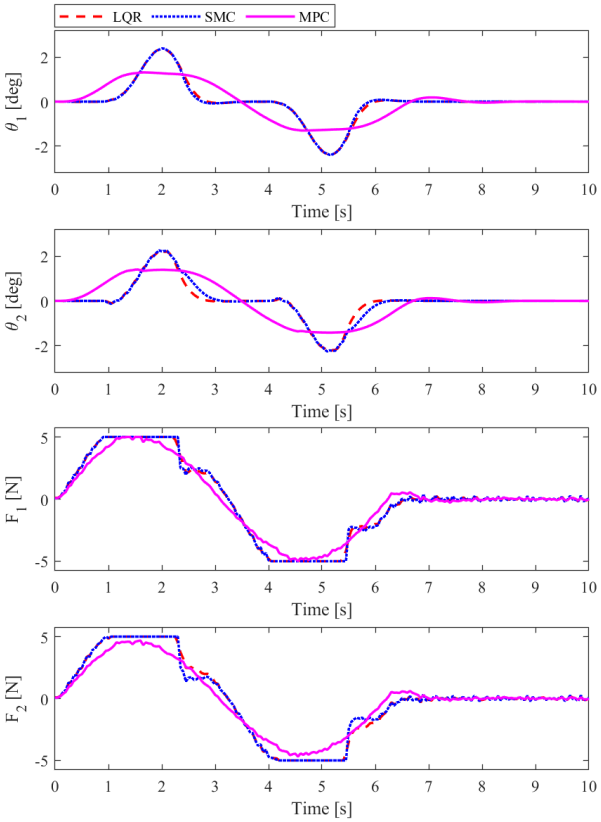

Figure 9. Simulation result of swing angle (θ_1, θ_2) and applied force (F_1, F_2) with increased m_m

magnitude of u, which only has a relatively minor impact on F_1, F_2 compared to the influence of acceleration compensation when mass is considerable.

The performance of these controllers, as illustrated in Figure 9 and Table 1 demonstrated how MPC accurately anticipates future saturation conditions and adjusts input magnitudes in advance to minimize the maximum swing angle. The forces applied are recorded in Figure 9, clearly highlighting that after the initiation of the simulation, both the LQR and SMC quickly reached their upper limits, consistently driving the MiC and hook with maximum output. As the trolley begins to decelerate, there is a sudden drop in force. In contrast, the output curve of the MPC remains smooth and continuous, demonstrating a more amicable interaction with the actuator. The results indicate that, while maintaining a similar overall RMSE, MPC exhibits a more conservative swing angle and is more actuator-friendly. This attribute makes MPC the most suitable proactive controller for MiC, which inherently carries a substantial load.

4 Conclusion

This study introduced a proactive hook-load stabilization system to address the inherent limitations of underactuated overhead cranes by adding two auxiliary inputs. With the focus on single-axis trolley motion along the jib, three Multiple-Input Multiple-Output (MIMO) controllers were compared in simulations, and the main outcomes are:

- Efficacy is verified through three comparative simulations, demonstrating superior performance against a control-less scenario.
- Resilience to uncertainty and undesired conditions is confirmed by considering factors like control signal delays, noisy sensor readings, and actuator saturation.

Results indicated the proposed MPC-based method enables more aggressive trolley motions, enhancing fault tolerance for novice operators and eventually maximizing operational efficiency.

Future works of this study involve conducting scaled experiments and observer design to enhance robustness under complex integrated disturbances. Meanwhile, the dimensionality of the system will be expanded to 3-D, considering the movement of the trolley in the complete horizontal plane.

References

[1] G. H. Kim and K. S. Hong. Adaptive sliding-mode control of an offshore container crane with unknown disturbances. *IEEE/ASME Transactions On Mechatronics*, 24(6):2850–2861, 2019. doi:10.1109/TMECH.2019.2946083.

[2] T. Yang, N. Sun, H. Chen, and Y. Fang. Adaptive optimal motion control of uncertain underactuated mechatronic systems with actuator constraints. *IEEE/ASME Transactions on Mechatronics*, 28(1):210–222, 2022. doi:10.1109/TMECH.2022.3192002.

[3] N. Sun, Y. Wu, Y. Fang, and H. Chen. Nonlinear antiswing control for crane systems with double-pendulum swing effects and uncertain parameters: Design and experiments. *IEEE Transactions on Automation Science and Engineering*, 15(3):1413–1422, 2017. doi:10.1109/TASE.2017.2723539.

[4] L. Ramli, Z. Mohamed, A. M. Abdullahi, H. I. Jaafar, and I. M. Lazim. Control strategies for crane systems: A comprehensive review. *Mechanical Systems and Signal Processing*, 95:1–23, 2017. doi:10.1016/j.ymssp.2017.03.015.

[5] B. Zhao, H. Ouyang, and M. Iwasaki. Motion trajectory tracking and sway reduction for double-pendulum overhead cranes using improved adaptive control without velocity feedback. *IEEE/ASME Transactions on Mechatronics*, 27(5):3648–3659, 2021. doi:10.1109/TMECH.2021.3126665.

[6] G. Li, X. Ma, Z. Li, and Y. Li. Time-polynomial-based optimal trajectory planning for double-pendulum tower crane with full-state constraints and obstacle avoidance. *IEEE/ASME Transactions on Mechatronics*, 28(2):919–932, 2022. doi:10.1109/TMECH.2022.3210536.

[7] T. Yang, N. Sun, H. Chen, and Y. Fang. Neural network-based adaptive antiswing control of an underactuated ship-mounted crane with roll motions and input dead zones. *IEEE Transactions on Neural Networks and Learning Systems*, 31(3):901–914, 2019. doi:10.1109/TNNLS.2019.2910580.

[8] H. Ouyang, J. Hu, G. Zhang, L. Mei, and X. Deng. Decoupled linear model and s-shaped curve motion trajectory for load sway reduction control in overhead cranes with double-pendulum effect. *Proceedings of the Institution of Mechanical Engineers, Part C: Journal of Mechanical Engineering Science*, 233(10):3678–3689, 2019. doi:10.1177/0954406218819029.

[9] H-H. Lee. Motion planning for three-dimensional overhead cranes with high-speed load hoisting. *International Journal of Control*, 78(12):875–886, 2005. doi:10.1080/00207170500197571.

[10] N. Sun, Y. Fang, Y. Zhang, and B. Ma. A novel kinematic coupling-based trajectory planning method for overhead cranes. *IEEE/ASME Transactions on Mechatronics*, 17(1):166–173, 2011. doi:10.1109/TMECH.2010.2103085.

[11] M. Zhang, Y. Zhang, B. Ji, C. Ma, and X. Cheng. Modeling and energy-based sway reduction control for tower crane systems with double-pendulum and spherical-pendulum effects. *Measurement and Control*, 53(1-2):141–150, 2020. doi:10.1177/0020294019877492.

[12] C. Aguiar, D. Leite, D. Pereira, G. Andonovski, and I. Škrjanc. Nonlinear modeling and robust lmi fuzzy control of overhead crane systems. *Journal of the Franklin Institute*, 358(2):1376–1402, 2021. doi:10.1016/j.jfranklin.2020.12.003.

[13] Y. Zhao and H. Gao. Fuzzy-model-based control of an overhead crane with input delay and actuator saturation. *IEEE Transactions on Fuzzy Systems*, 20(1): 181–186, 2011. doi:10.1109/TFUZZ.2011.2164083.

[14] R. Roman, R. Precup, and E. M. Petriu. Hybrid data-driven fuzzy active disturbance rejection control for tower crane systems. *European Journal of Control*, 58:373–387, 2021. doi:10.1016/j.ejcon.2020.08.001.

[15] M. Vukov, W. Van Loock, B. Houska, H. J. Ferreau, J. Swevers, and M. Diehl. Experimental validation of nonlinear mpc on an overhead crane using automatic code generation. In *2012 American Control Conference (ACC)*, pages 6264–6269. IEEE, 2012. doi:10.1109/ACC.2012.6315390.

[16] D. Schindele and H. Aschemann. Fast nonlinear mpc for an overhead travelling crane. *IFAC proceedings volumes*, 44(1):7963–7968, 2011. doi:10.3182/20110828-6-IT-1002.03510.

[17] P. Bauer and J. Bokor. Performance comparison of siso and mimo low-level controllers in a special trajectory tracking application. In *22nd Mediterranean Conference on Control and Automation*, pages 1293–1298. IEEE, 2014. doi:10.1109/MED.2014.6961554.

[18] H. Chen, Y. Fang, and N. Sun. A swing constraint guaranteed mpc algorithm for underactuated overhead cranes. *IEEE/ASME Transactions on Mechatronics*, 21(5):2543–2555, 2016. doi:10.1109/TMECH.2016.2558202.

[19] H. Chen and N. Sun. Nonlinear control of underactuated systems subject to both actuated and unactuated state constraints with experimental verification. *IEEE Transactions on Industrial Electronics*, 67(9): 7702–7714, 2019. doi:10.1109/TIE.2019.2946541.

[20] J. Vaughan, D. Kim, and W. Singhose. Control of tower cranes with double-pendulum payload dynamics. *IEEE Transactions on Control Systems Technology*, 18(6):1345–1358, 2010. doi:10.1109/TCST.2010.2040178.

[21] J. A. E. Andersson, J. Gillis, G. Horn, J. B. Rawlings, and M. Diehl. CasADi – A software framework for nonlinear optimization and optimal control. *Mathematical Programming Computation*, 11(1):1–36, 2019. doi:10.1007/s12532-018-0139-4.